We are IntechOpen, the world's leading publisher of Open Access books Built by scientists, for scientists

4,800
Open access books available

122,000
International authors and editors

135M
Downloads

Our authors are among the

154
Countries delivered to

TOP 1%
most cited scientists

12.2%
Contributors from top 500 universities

CLARIVATE ANALYTICS BOOK CITATION INDEX INDEXED

WEB OF SCIENCE™

Selection of our books indexed in the Book Citation Index in Web of Science™ Core Collection (BKCI)

Interested in publishing with us?
Contact book.department@intechopen.com

Numbers displayed above are based on latest data collected.
For more information visit www.intechopen.com

Chapter 8

ZnO/Sepiolite Catalysts – Characterization and Photoactivity Measurements

A. Neren Ökte

Additional information is available at the end of the chapter

http://dx.doi.org/10.5772/61973

Abstract

Sepiolite-supported ZnO catalysts (ZnO-SEP) were prepared and characterized using X-ray diffraction (XRD), surface area (BET) measurements, scanning electron microscopy (SEM) with energy-dispersive X-ray analysis (EDX), X-ray photoelectron spectroscopy (XPS) and UV-vis diffuse reflectance spectra (UV-vis DRS) techniques. XRD analysis supplied information about the generation of ZnO nanoparticles. SEM images and elemental mapping scans revealed variations in the surface morphology of the SEP after ZnO loading. Supported catalysts possessed higher surface areas and pore volumes in comparison to unsupported catalyst (0.25 M ZnO). They also revealed suitable band-gap energies in the UV-A region. XPS analysis confirmed the build-up of ZnO nanoparticles on the SEP matrix with the form of Zn^{2+} oxidation state. Photocatalytic performances were evaluated in terms of methyl orange (MO) decolorization process following pseudo-first-order kinetics. The repeatability of photocatalytic activity was also tested.

Keywords: Sepiolite, ZnO, Supported catalysts, Methyl orange

1. Introduction

The complete degradation of dye molecules is not possible by the application of precipitation, adsorption, oxidation, reduction and biological and electrochemical types of conventional methods. These methods may either end up with less efficiency or create a secondary sludge. Semiconductor photocatalysis is an advanced oxidation process (AOP) for the treatment of air and water streams and emerged as an important technology for the degradation of dye molecules. In summary, the mechanism of photocatalytic processes is initiated by the band-gap illumination and this leads to production of electron-hole pairs. After separation, electrons and holes migrate to the catalyst surface, induce redox reactions with adsorbed pollutants and eventually result in the degradation of the dye pollutants.

ZnO is a wide band-gap (~3.3 eV) semiconductor that has been extensively used because of its catalytic and photochemical properties along with its low cost [1]. There are many reports of ZnO having higher photocatalytic activities than other semiconductors in both air and aqueous media [2,3]. As a photocatalyst, the surface area plays an important role since reactions mainly occur between catalyst surfaces and pollutants. The nanoscale ZnO crystals have shown larger surface areas and higher photocatalyic performances than that of bulk materials [4]. Therefore, recent studies have focused on the synthesis of nanostructured ZnO with tunable size and shape [5,6]. However, ZnO nanoparticles are not stable in acidic and alkaline conditions and also show rapid deactivation in bulk due to increased tendency of aggregation [7]. Hence, the development of industrially viable, cost-effective, eco-friendly adsorbents with attractive multiple functions such as adsorption, and decomposition becomes important. Silicate adsorbents engineered with photocatalytic ingredients, for example, tailoring the aluminosilicate layers and their surfaces with nanostructured semiconducting photocatalysts, can make them multifunctional composites and heterogeneous catalysts [8]. ZnO/clay system reveals the potential of this composite for various applications [9–12]. Among clay minerals, the usage of sepiolite as a support material is rarely reported [13–18]. Natural sepiolite is a very cheap, fibrous and hydrated magnesium silicate with a relatively high surface area. The presence of alkalescent [MgO_6] and acidic [SiO_4] centers in the sepiolite structure enhances the adsorption of reactant molecules and their degradation possibility. Moreover, silicate layers appear as an attractive support for the assembly of small-sized metals and metal-oxide aggregates (clusters and nanoparticles) that have been mainly employed for catalytic purposes. The immobilization of nanoparticles on the inner and outer surfaces of inorganic supports results in the formation of nanocomposite materials. The synergy established among nanoparticles and support systems makes them attractive options for the degradation of pollutants. In the study of Xu et al., quantum-sized ZnO particles supported on sepiolite were prepared using a sol-gel method with the sepiolite of acid activation as carrier and zinc acetate dihydrate ($Zn(CH_3COO)_2\ 2H_2O$) and lithium hydroxide monohydrate ($LiOH\ H_2O$) as raw materials [13]. They found that the nano-ZnO supported on sepiolite can not only solve the dispersing problem but also has a positive synergistic effect on the ZnO photocatalysis. Bautista et al. prepared TiO_2-Sep supports of vanadium oxide in order to obtain a new TiO_2 support with a high and thermostable surface area [14]. According to this study, vanadium oxides supported on TiO_2-coated sepiolite and sepiolite characterization studies indicated that well-dispersed vanadium in both types of supports was achieved in the systems with vanadia loading below the theoretical monolayer. Above this vanadia loading, the formation of V_2O_5 nanoparticles with a mainly crystalline character took place as well as the formation of V-Mg mixed metal-oxide phases, especially in systems supported on sepiolite. The hydrophilic character and more open structure of the sepiolite was underlined in the study of Arques et al. [15]. Accordingly, sepiolite appeared to be a convenient support for pyrylium salts to be employed as a heterogeneous solar photocatalyst. Also, promising results have been obtained testing the performance of the new material with ferulic acid as target pollutant, and important percentages of photo-oxidation were achieved. In another study, monolithic catalysts based on Rh/TiO_2-sepiolite were developed and tested in the decomposition of N_2O traces [16]. The system was found to be extremely sensitive to the amount of rhodium and is an attractive alternative for the elimination of N_2O traces from stationary sources due to the combination of high catalytic activity with a low pressure drop and optimum textural/mechanical properties. The structural and photoca-

http://dx.doi.org/10.5772/61973

talytic properties of TiO_2-supported sepiolite and sodium ion-treated sepiolite catalysts were also investigated for the degradation of β-naphthol molecule [17]. Sodium chloride treatment enhanced the attraction of sepiolite support through TiO_2 nanoparticles. This study explored that sepiolite can be employed as a catalyst support for the photocatalytic degradation reactions in solution. Such supported catalysts can be readily separated from the suspension without filtration since they decant in minutes, while TiO_2 (Degussa P-25) sample could not sediment over hours. This provided an important, practical advantage in the usage of TiO_2-supported sepiolite catalysts.

In this chapter, a mixed structure of ZnO and sepiolite (ZnO-SEP) is examined for the degradation of an azo dye, methyl orange (MO). Such supported catalyst systems are prepared using a coprecipitation method with highly dispersed active ZnO nanoparticles and investigated in terms of the dark adsorption capacities and photoactivities. X-ray diffraction (XRD), surface area (BET) measurements, scanning electron microscopy (SEM) with energy-dispersive X-ray analysis (EDX), X-ray photoelectron spectroscopy (XPS) and UV-vis diffuse reflectance spectra (UV-vis DRS) techniques are used for the characterization of these catalysts. The decolorization of MO is followed under UV irradiation.

2. Experimental section

The raw SEP used as a support in this study was obtained from the Eskişehir region of Anatolia (Turkey) and characterized by X-ray diffraction and SEM-EDX analyses. The chemical composition was found as SiO_2 (69.25%), MgO (28.92%), Al_2O_3 (1.12%), Na_2O (0.55%) and TiO_2 (0.16%). The clay was ground to approximately 200-mesh size powder. Zinc nitrate hexahydrate ($Zn(NO_3)_2$ $6H_2O$) (99.0%, Merck), sodium carbonate (Na_2CO_3) (analytical grade, Merck) and (4-[[(4-dimethylamino)phenyl]-azo]benzenesulfonic acid sodium salt] (methyl orange, Merck) were used as provided by the suppliers without further purification. Deionized water, purified with an Elga-Pure Water Purification (UHQ II) system, was used for preparing solutions in the experiments.

The following procedures and techniques were applied for the synthesis and characterization of the photocatalysts:

ZnO catalysts in the absence of SEP were prepared by a coprecipitation method using $Zn(NO_3)_2$ $6H_2O$ and Na_2CO_3 precursors [19]. Briefly, the precursors with 0.25 M concentrations were separately dissolved in deionized water. Then, 100 mL of $Zn(NO_3)_2$ $6H_2O$ were added gradually to 100 mL of Na_2CO_3 solution under continuous stirring. The resulting white suspension was stirred for 2 h at room temperature followed by several washings and centrifugations at 4000 rpm. Then, the resulting precipitate was dried at 100°C for 12 h and calcined at 500°C with a heating rate of 10°C min^{-1} for 5 h. Finally, the catalysts were ground into fine powder and named as 0.25 M ZnO.

Depending on the loading of ZnO on the support, precursor concentrations as 0.125 M ZnO, 0.25 M ZnO or 0.5 M ZnO (prepared following the above procedure) were added to the SEP solution. After stirring the mixed suspension for about 12 h at room temperature, several

washings and centrifugations (at 4000 rpm) were applied. The resulting catalysts were dried at 100°C for 12 h and then calcined at 500°C with a rate of 10°C min^{-1} for 5 h. Finally, the catalysts were ground into fine powder and named as 0.125 M ZnO-SEP, 0.25 M ZnO-SEP and 0.5 M ZnO-SEP.

X-ray diffraction was used to monitor the formation of crystal planes and measure the crystalline size of ZnO nanoparticles. The analyses were recorded on a Rigaku-D/MAX-Ultima diffractometer using Cu-Kα radiation (λ=1.54 Å) operating at 40 kV and 40 mA and scanning rate of 2 min^{-1}. Nitrogen sorption analysis was used to measure the surface areas, pore volumes and pore diameters of the catalysts.

The nitrogen adsorption/desorption isotherms were obtained at 77 K using Quantachrome Nova 2200e automated gas adsorption system. The specific surface areas were determined using multi-point BET analysis and the pore sizes were measured by the BJH method of adsorption.

The surface morphologies were determined using scanning electron microscopy (SEM) in combination with energy-dispersive X-ray analysis on an ESEM-FEG/EDAX Philips XL-30 instrument operating at 20 kV. The catalysts were fixed with carbon tape prior to the metallization process with gold (Sputter Coater-Balzer SCD050).

In X-ray photoelectron spectroscopy (XPS) tests, Thermo Scientific K-Alpha X-ray photoelectron spectrometer equipped with electron analyzer and Al-Kα micro-focused monochromator was used. The areas of peaks were estimated by calculating the integral of each peak after subtracting a Shirley background and fitting the experimental curve to a combination of Lorentzian/Gaussian lines. Binding energy shifts were observed in the samples and the instrument was calibrated using the carbon peak (C-1s) at 285 eV as in the other studies [20,21].

The UV-vis diffuse reflectance spectra (UV-vis DRS) of the supports, 0.25 M ZnO and supported catalysts were obtained using UV-vis spectrophotometer (UV-2450, Shimadzu) equipped with an integrating sphere reflectance accessory. The baseline correction was done by $BaSO_4$. The spectra were recorded in the range 200–600 nm for the catalysts and the FA using $BaSO_4$ as a reference.

For the photocatalytic experiments, the details of reaction systems were given in our previous studies [22,23]. Briefly, a Pyrex flask reactor was located in an "irradiation box" equipped with eight black light lamps (Philips TL 15W/5BLB) with an emission maximum at λ=365 nm. The lamps were positioned to surround the flask with an incident photon flux of 4.7×10^{15} photons s^{-1}. Then, 0.2 g of catalysts with 200 mL of 3.27 mg L^{-1} MO (unless the concentration effect of MO was controlled) was used as reaction solutions. The flask had an inlet for the air circulation and an outlet for the collection of aliquots. Prior to irradiation, suspensions were magnetically stirred in the dark for 30 min. UV-vis spectrophotometer (UV-2450, Shimadzu) was used to monitor the absorbance spectra of MO at 464 nm as a function of irradiation time. All experiments were performed at room temperature and without concerning the degradation intermediates. Also, measurements were conducted at least twice and the average value was recorded. MO decolorization percentages were calculated by the following equation:

http://dx.doi.org/10.5772/61973

$$\text{Decolorization } \% = \frac{C_0 - C}{C_0} \times 100$$

where C_0 is the initial concentration of MO and C is the concentration of MO after "t" minutes irradiation.

3. Results and discussion

3.1. Characterization of ZnO-SEP catalysts

3.1.1. XRD analysis

The phase identification of the raw SEP and the supported catalysts were performed by XRD analysis from 0° το 70° (2θ) (Figure 1). The characteristic d 110 reflection of the SEP was noticed with a basal spacing of 12.19 Å at 7.24° (2θ). ZnO loadings decrease the intensities of all SEP reflections. For the supported catalysts, alteration in ZnO concentrations did not modify the position of the SEP peaks due to the non-expandable nature of the SEP. Supported catalysts also exhibited wurtzite ZnO structure with d 100, d 002, d 101, d 102, d 110, d 103 and d 200 crystal planes at 31.9°, 34.6°, 36.4°, 47.7°, 56.7°, 63.1° and 66.6° (2θ), respectively. The broad and less intense ZnO peaks got sharper and more intense with the increments in ZnO loadings.

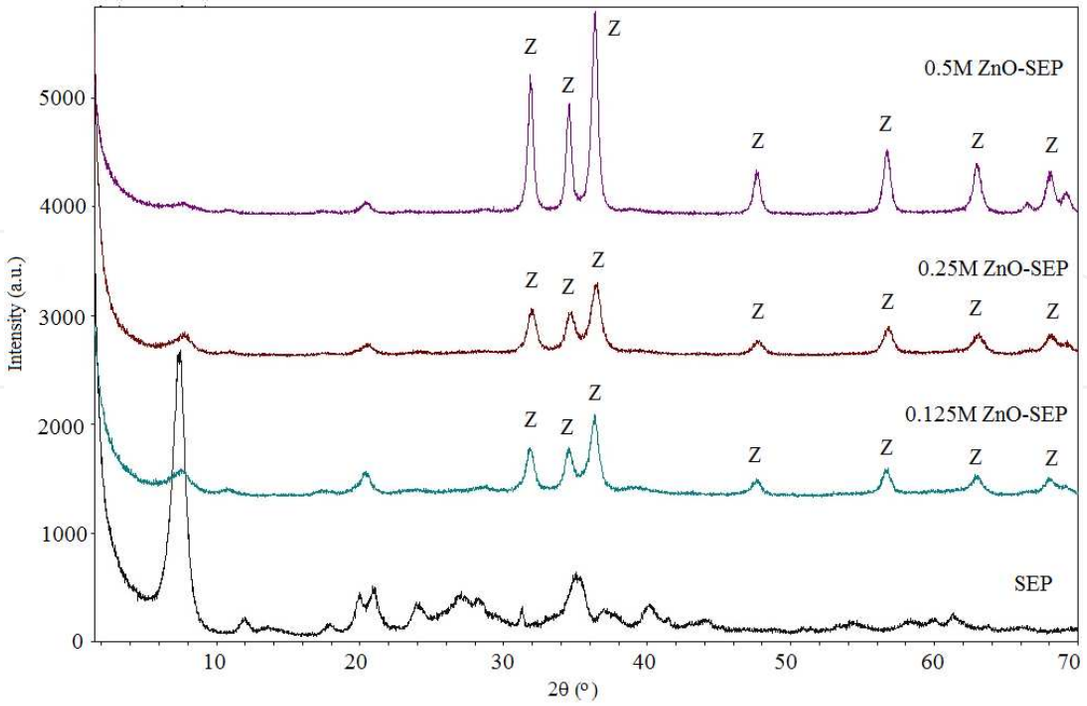

Figure 1. XRD patterns of SEP and supported catalysts (Z: ZnO).

The crystalline sizes (D_{ZnO}) calculated using Scherrer's equation for the broadening of d 101 reflection of ZnO were found as 16.1 nm (for 0.25 M ZnO), 13.4 nm (for 0.125 M ZnO-SEP), 12.3 nm (for 0.25 M ZnO-SEP) and 15.1 nm (for 0.5 M ZnO-SEP) (Table 1). The reduction in the ZnO crystalline sizes and the decrements in the intensities of SEP reflections may suggest highly dispersed ZnO nanoparticles over the surface and bulk.

Catalysts	D_{ZnO} (nm)[a]	BET (m^2 g^{-1})[b]	V_{pore} (cm^3 g^{-1})[c]	R_{pore} (Å)[d]
0.25M ZnO	16.1	7.58	0.012	17.7
SEP	-	104.5	0.140	14.9
0.125M ZnO-SEP	13.4	91	0.151	19.1
0.25M ZnO-SEP	12.3	47	0.077	20.2
0.5M ZnO-SEP	15.1	51	0.091	14.8

a Calculated from the (101) diffraction peak of ZnO using the Scherrer equation.
b Determined from nitrogen adsorption-desorption isotherms using BET equation.
c Determined from cumulative adsorption pore volume using BJH method.
d Determined from adsorption pore size using BJH method.

Table 1. Crystalline sizes (D_{ZnO}), surface areas (BET), total pore volumes (Vpore) and pore radius (Rpore) of 0.25 M ZnO, SEP and supported catalysts.

3.1.2. Nitrogen adsorption desorption isotherms

The textural characterization points out that 0.25 M ZnO had type II isotherms, which refer to non-porous materials (Figure 2A and 2B). However, the raw SEP and the supported catalysts had type IV nitrogen adsorption-desorption isotherms typical of mesoporous structures with hysteresis loops [24]. Almost similar pore radius was detected for all catalysts and the SEP (Table 1). The capillary condensation taking place within the mesopores in the high P/P_0 range became more difficult with the formation of narrower loops, owing to the higher ZnO loading concentrations. Accordingly, 0.125 M ZnO-SEP shows almost similar surface area and pore volume with respect to the SEP, whereas 0.25 M ZnO-SEP and 0.5 M ZnO-SEP reveal lower values. The partial blockage of the pores by the ZnO nanoparticles on the supports' surface sites, edges and corners was expected to induce an easier attraction among MO molecules and the catalyst particles.

3.1.3. SEM (EDX) analysis

Figure 3 illustrates the SEM and elemental mapping images of 0.25 M ZnO-SEP. The characteristic fibrous structure of SEP and pseudo-spherical shape of the as-prepared ZnO catalyst were reported previously [17,22]. The heterogeneously dispersed ZnO nanoparticles within the SEP matrix resulted in a different morphology in comparison to the raw SEP and unsupported catalyst. In the EDX analysis of 0.25 M ZnO-SEP (not shown), the reduction in the peak intensities and percentages of SiO_2 and MgO (from 69.25% to 16.08% for SiO_2 and from 28.92% to 10.93% for MgO) and also simultaneous detection of ZnO peak signified the in situ build-

http://dx.doi.org/10.5772/61973

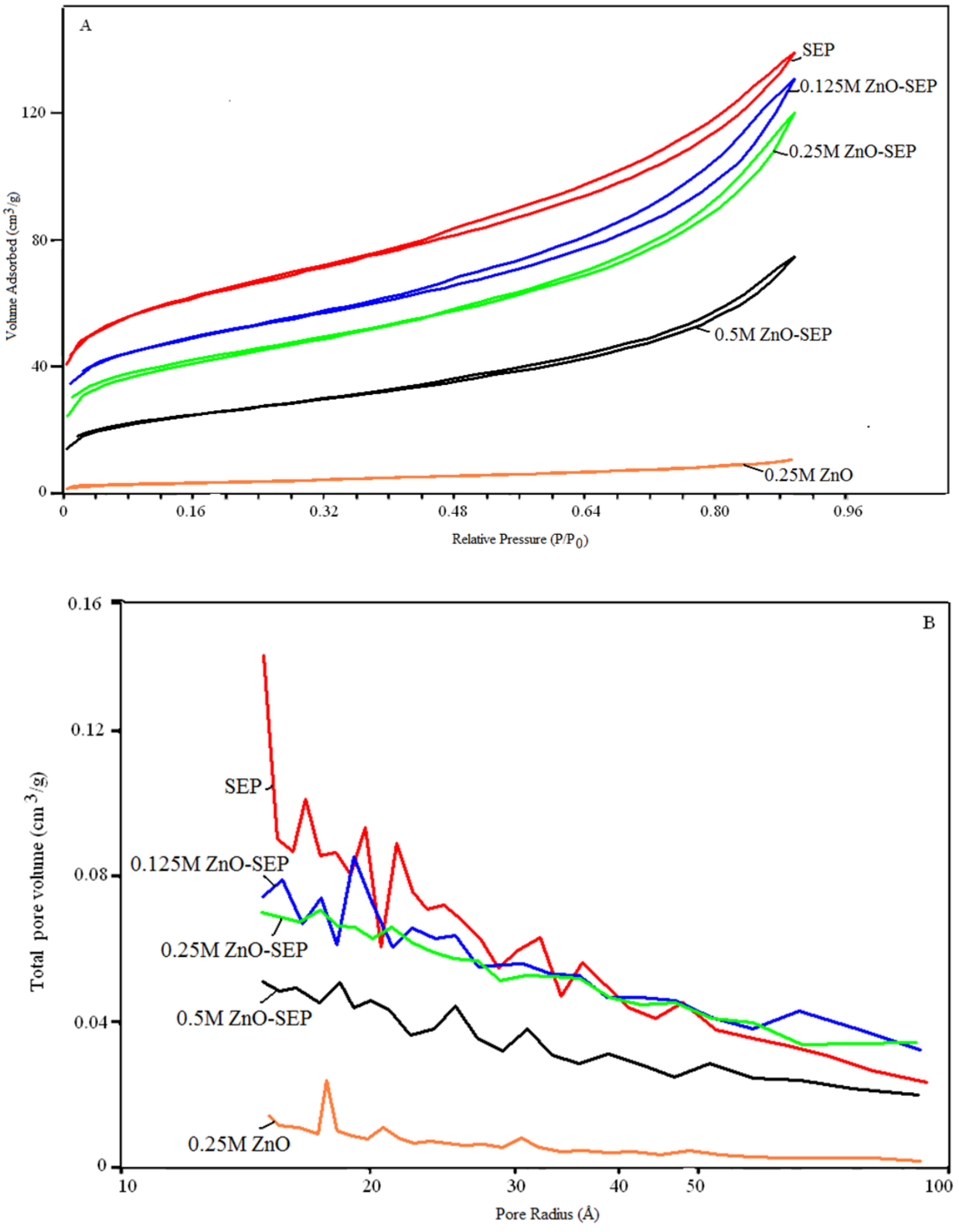

Figure 2. (A) Nitrogen adsorption/desorption isotherms and (B) pore size distribution plots of 0.25 M ZnO, SEP and supported catalysts.

up of ZnO nanoparticles in the SEP structure. In mapping images, ZnO existence was proven by the dominating Zn signals within less dense regions of Si and Mg constituents.

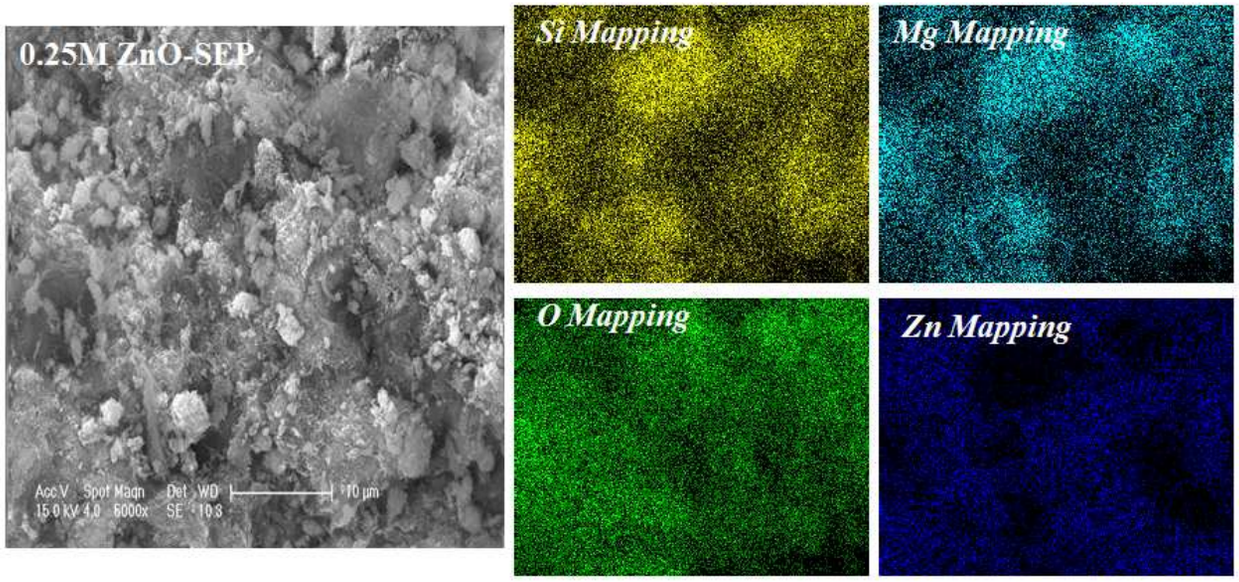

Figure 3. SEM and mapping images of 0.25 M ZnO-SEP.

3.1.4. XPS analysis

In order to control the presence of ZnO on the SEP host, the surface chemical composition was analyzed by the XPS method, focusing in particular on the binding energies of the typical lines of Zn and O (Figure 4). The survey scan of 0.5 M ZnO-SEP reveals Zn peaks in addition to the Mg (49.5 eV), Al (75.6 eV), Si (103 eV), O (531.47 eV) and some Auger peaks of the SEP (Figure 4A). Figure 4B depicts the presence of Zn ion with a doublet matching to Zn 2p3/2 and 2p1/2 core levels (Figure 4B). This shows the presence of Zn^{2+} ions in an oxide environment [25,26]. The O1s photoelectron peak is deconvoluted by three subspectral parts (Figure 4C). The peak at 527 eV is attributed to the lattice oxygen in a Zn-O-Zn network with 8.7% spectral area. The shift in the peak position with respect to ZnO binding energy of 530.5 eV can be due the complex configuration in the ZnO-SEP matrix. For the other two components, 64.7% spectral area refers to MgO and Al_2O_3 at 531 eV and 26.5% spectral area corresponds to SiO_2 at 532.81 eV.

3.1.5. UV-vis DRS analysis

UV-vis absorption spectroscopies of the SEP and supported catalysts are presented in Figure 5A. The raw SEP shows an extended profile in between 200 and 600 nm. In contrast, 0.25 M ZnO reveals its distinctive edge below 400 nm. The supported catalysts resemble this characteristic edge, which is more pronounced for the catalyst having the highest ZnO concentration. The UV activities of the supported catalysts are evidenced by the evaluated band-gap energies based on Kubelka-Munk transformed reflectance spectra as 3.08 eV for 0.125 M ZnO-SEP, 3.09 eV for 0.25 M ZnO-SEP and 3.16 eV for 0.5 M ZnO-SEP (Figure 5B).

http://dx.doi.org/10.5772/61973

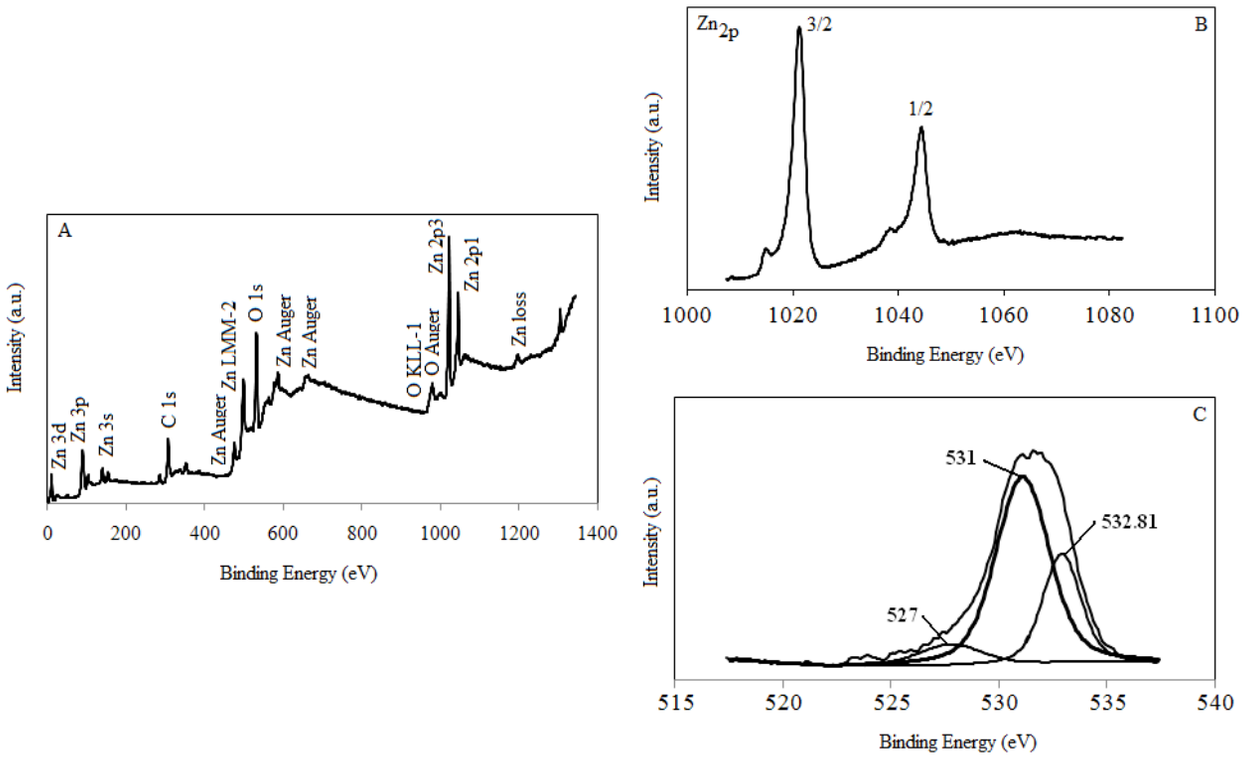

Figure 4. XPS analysis of 0.5 M ZnO-SEP: (A) survey spectrum, (B) Zn 2p spectra and (C) O 1s spectra.

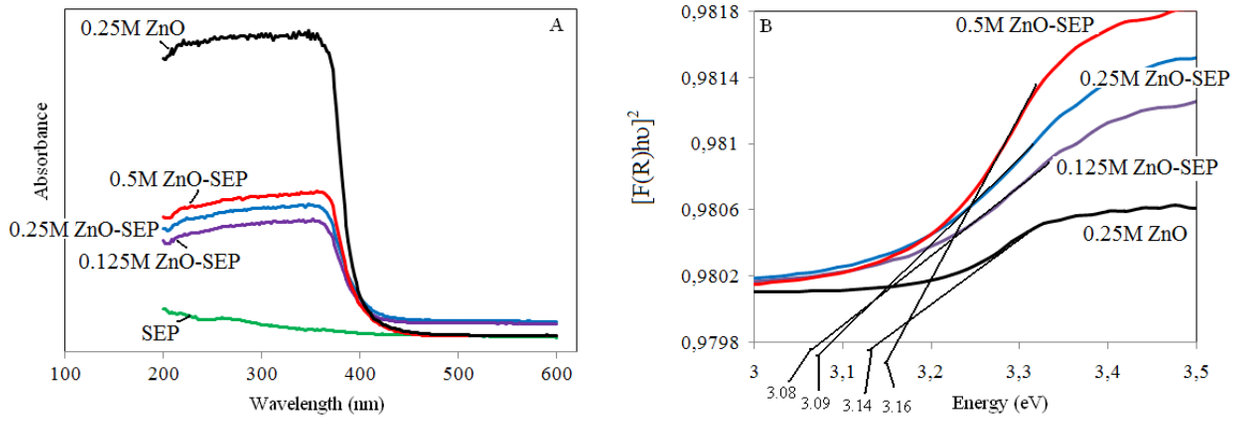

Figure 5. A) Diffuse reflectance spectra of SEP, 0.25 M ZnO and supported catalysts and (B) Kubelka-Munk transformed reflectance spectra of 0.25 M ZnO and supported catalysts.

3.2. Decolorization of MO by ZnO-SEP catalysts

Control experiments were performed under dark conditions for 0.25 M ZnO and 0.25 M ZnO-SEP (Figure 6). The remaining MO percentage was found as 83% in the presence of 0.25 M ZnO after 60 min, and then no significant variation was detected. The supported catalyst, however, shows a lower percentage (73%) in 80 min. The interaction between the SEP matrix and ZnO

nanoparticles facilitated the adsorption of MO molecules. The low isoelectric point of the SEP (IEP_{SEP}~2) increased the contact possibility of positively charged Zn^{2+} ions or ZnO (with high isoelectric point ~9) [18]. The attraction between positively charged Zn^{2+} ions and negatively charged MO moiety decreased the intensity of absorption band at 464 nm, which is responsible from the destruction of the chromophoric (-N=N-) group. The negligible photolysis of MO proves the active role of ZnO nanoparticles within the supported catalyst system. It is also noted that the raw SEP does not participate in the decolorization of MO (not shown).

The photoactivities of the supported catalysts were examined under irradiation (Figure 6, inset). The highest MO remaining percentage (43%) was obtained in the presence of 0.125 M ZnO-SEP within 120 min. The percentage of MO decreased upon the loading concentration of ZnO. The synergy established on the mixed structures of ZnO and SEP improved the catalyst performance. Accordingly, 0.5 M ZnO-SEP shows the best activity with the lowest MO remaining percentage (19.8%) in solution.

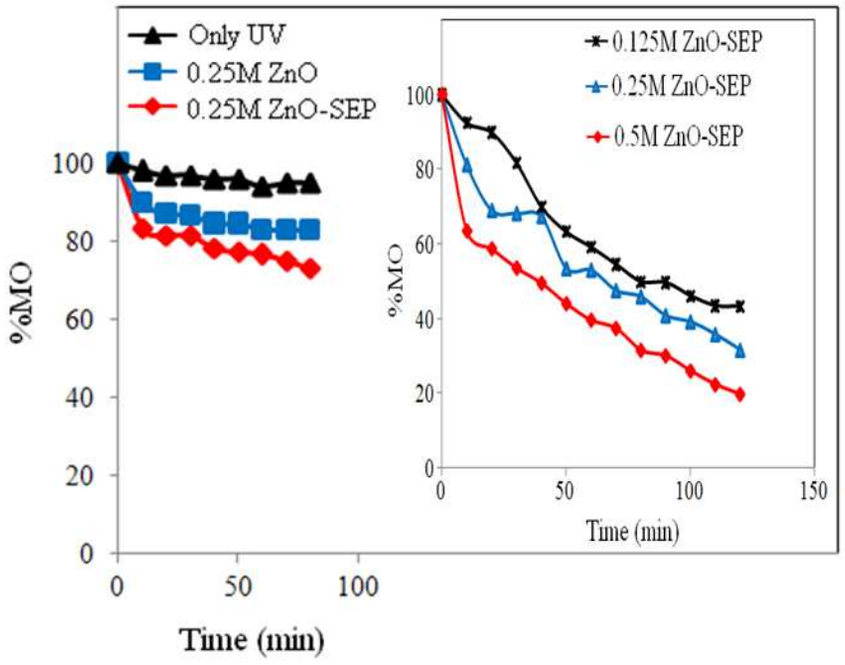

Figure 6. Photolysis and dark adsorption experiments. Inset: Photocatalytic activities of the supported catalysts.

The whole mechanism starts with the illumination of ZnO nanoparticles and production of electron-hole pairs (Eq. (1)).

$$ZnO + h\gamma(UV) \rightarrow e_{CB}^{-} + h_{VB}^{+} \quad (1)$$

The main active species in such processes are known as h_{vb}^{+}, $^{\cdot}OH$ and $O_2^{\cdot-}$ [27,28]. The radicals may form either by the reactions of photogenerated holes or electrons. The photogenerated electron (e_{cb}^{-}) can be easily transferred to the O_2 molecules promoting the $O_2^{\cdot-}$ formation and

http://dx.doi.org/10.5772/61973

then converted to the active $^{\cdot}OH$ via hydrogen peroxide and hydroperoxyl radical generations (Eqs. (2)–(5)).

$$O_2 + e^- \rightarrow O_2^{\bullet -} \quad (2)$$

$$O_2^{\bullet -} + H^+ \rightarrow HO_2^{\bullet} \quad (3)$$

$$2HO_2^{\bullet} \rightarrow H_2O_2 + O_2 \quad (4)$$

$$H_2O_2 + O_2^{\cdot -} \rightarrow {}^{\bullet}OH + O_2 + OH^- \quad (5)$$

At the same time, the photogenerated h_{vb}^+ can be captured on the catalyst surface undergoing charge transfer with adsorbed water molecules or with surface-bound hydroxide species to generate active $^{\cdot}OH$ (Eqs. (6) and (7)) and results in the degradation of MO molecule (Eq. (8)).

$$h_{vb}^+ + H_2O \rightarrow H^+ + {}^{\bullet}OH \quad (6)$$

$$h_{vb}^+ + OH^- \rightarrow {}^{\bullet}OH \quad (7)$$

$${}^{\bullet}OH + MO \rightarrow MO\ (\text{decolorization and degradation}) \quad (8)$$

Thus, the separation of the charge carriers also enhanced the yield of hydroxyl radicals (highly reactive electrophilic oxidants) and improved the photocatalytic activity of the supported catalysts. The addition of the hydroxyl radical to the double bond of the azo group is referred to as the main reaction pathway, with the disappearance of the color. The second route followed the addition of hydroxyl radical to the aromatic rings [29,30]. Alternatively, hydroxyl radicals may attack the carbon atom bearing the azo bond [30]. Further attacks caused the formation of sulfonated intermediates, aromatic amine and phenolic compounds and ring open fragments [31].

Kinetic analysis was performed by varying the initial MO concentration from 16.2 to 3.27 mg L^{-1} in the presence of 0.5 M ZnO-SEP (not shown). The linearity obtained between $\ln(C_0/C)$ versus t plot indicates pseudo-first-order kinetics, where C_0 is the initial concentration of MO (mg L^{-1}) and C is the concentration of MO (mg L^{-1}) at irradiation time t (min) (Figure 7). The rate constants k (min^{-1}) hence calculated (slopes of the lines) were found to decrease with increasing concentration of MO (from 0.01 (3.27 mg L^{-1}) to 0.005 min^{-1} (16.2 mg L^{-1})). This can be a result of blocking of the photocatalytically active sites on the supported catalyst and reducing the interaction of photons with these sites.

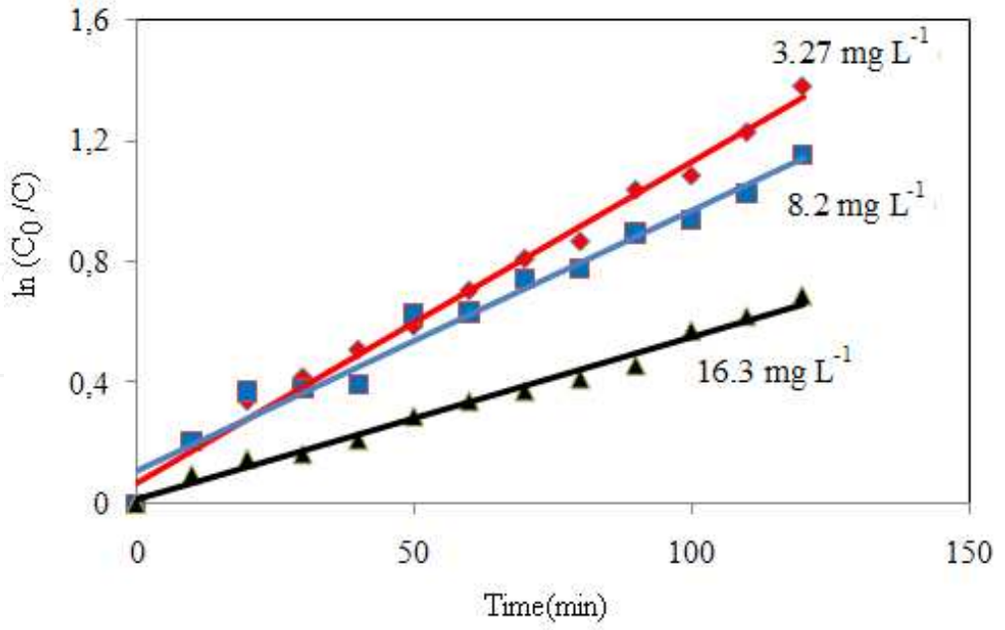

Figure 7. Effect of initial MO concentration on the photoactivity of 0.5 M ZnO-SEP.

The stability of 0.5 M ZnO-SEP catalyst was examined by recycling experiments (Figure 8). For each run, 0.5 M ZnO-SEP was filtrated, washed and calcined at 500°C for 2 h. After four cycles, the percentage of MO remaining in solution was found to increase by only approximately 3% (from 19.8% to 22%). The slight increment in the percentage can be attributed to the catalyst loss during each collection and rinsing steps.

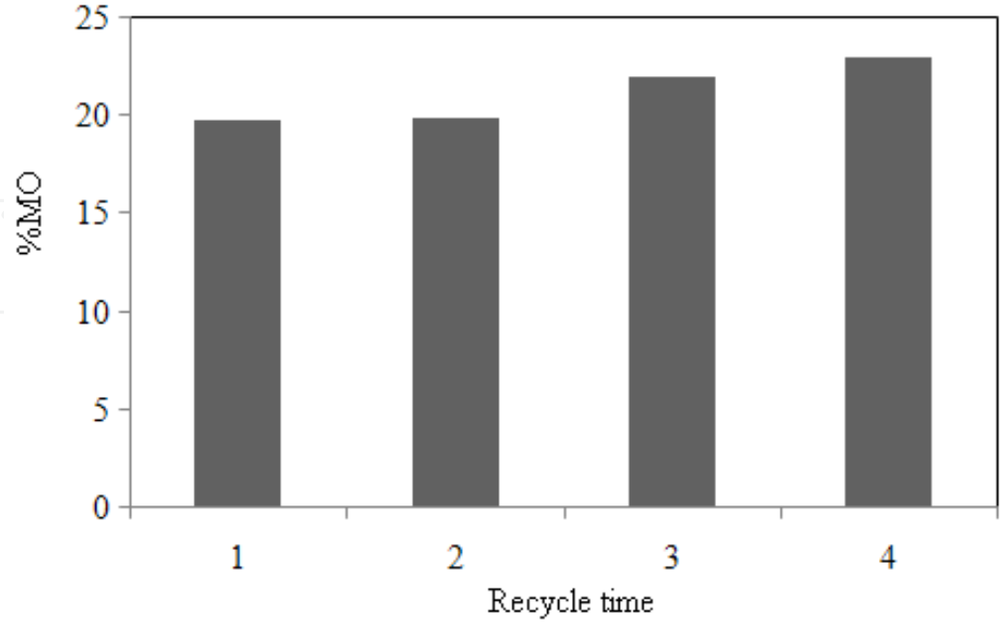

Figure 8. Reuse properties of 0.5 M ZnO-SEP.

http://dx.doi.org/10.5772/61973

4. Conclusions

This chapter has summarized the recent study of the author in an attempt to learn more about supported catalyst framework where clay mineral sepiolite is used as a support material for ZnO nanocatalysts. These photocatalysts were prepared and characterized by XRD, BET, SEM (EDX), XPS and DRUV techniques. EDX, mapping and XPS analysis evidence the existence of ZnO nanoparticles. D_{ZnO} sizes do not exhibit significant differences depending on the ZnO loading concentrations. Moreover, supported catalysts exhibit an absorption edge similar to 0.25 M ZnO. The pronounced performance of the supported catalysts is attributed to the highly dispersed ZnO nanoparticles within the ZnO-SEP matrix. Also, such systems can be readily separated from the suspension without filtration, providing an important, practical advantage in the usage of sepiolite supported catalysts.

Future studies will focus on the synthesis of new supported catalyst systems and their applications in energy and environmental issues.

Acknowledgements

This study was supported by the Boğaziçi University Research Foundation (Project No. 14B05P11/8820).

Author details

A. Neren Ökte*

Address all correspondence to: okteayse@boun.edu.tr

Department of Chemistry, Boğaziçi University, Bebek, Istanbul, Turkey

References

[1] Lam S. M., Sin J. C., Abdullah A. Z., Mohamed A. R., Degradation of wastewaters containing organic dyes photocatalysed by zinc oxide: A review. Desalin. Water Treat. 2012; 41: 131–169. DOI: 10.1080/19443994.2012.664698

[2] Kansal S. K., Ali A. H., Kapoor S., Photocatalytic decolorization of beibrich scarlet dye in aqueous phase using different nanophotocatalysts. Desalination. 2010; 259: 147–155. DOI: 10.1016/j.desal.2010.04.017

[3] Wahab R., Tripathy S. K., Shin H. S., Mohapatra M., Musarrat J., Al-Khedhairy A. A., Kaushik N. K., Photocatalytic oxidation of acetaldehyde with ZnO-quantum dots. Chem. Eng. J. 2013; 226: 154–160. DOI: 10.1016/j.cej.2013.02.128

[4] Kajbafvala A., Ghorbani H., Paravar A., Samberg J. P., Kajbafvala E., Sadrnezhaad S. K., Effects of morphology on photocatalytic performance of zinc oxide nanostructures synthesized by rapid microwave irradiation methods. Superlattice Microst. 2012: 51: 512–522. DOI: 10.1016/j.spmi.2012.01.015

[5] Sin J. C., Lam S. M., Lee K. T., Mohamed A. R., Preparation and photocatalytic properties of visible light-driven samarium-doped ZnO nanorods. Ceram. Int. 2013; 39: 5833–5843. DOI: 10.1016/j.ceramint.2013.01.004

[6] Lam S. M., Sin J. C., Abdullah A. Z., Mohamed A. R., Green hydrothermal synthesis of ZnO nanotubes for photocatalytic degradation of methylparaben. Mater. Lett. 2013; 93: 423–426. DOI: 10.1016/j.matlet.2012.12.008

[7] Mihai G. D., Meynen V., Mertens M., Bilba N., Cool P., Vansant E. F., ZnO nanoparticles supported on mesoporous MCM-41 and SBA15: a comparative physicochemical and photocatalytic study. J. Mater. Sci. 2010; 45: 5786–5794. DOI: 10.1007/s10853-010-4652-8

[8] Mahesh K. P. O., Kuo D. H., Huang B. R., Facile synthesis of heterostructured Ag-deposited SiO_2@TiO_2 composite spheres with enhanced catalytic activity towards the photodegradation of AB 1 dye. J. Mol. Catal. A: Chem. 2015; 396: 290–296. DOI: 10.1016/j.molcata.2014.10.017

[9] Németh J., Rodríguez-Gattorno G., Díaz D., Vázquez-Olmos A. R., Dékány I., Synthesis of ZnO nanoparticles on a clay mineral surface in dimethyl sulfoxide medium. Langmuir. 2004; 20: 2855–2860. DOI: 10.1021/la035097s

[10] Hur S. G., Kim T. W., Hwang S. J., Hwang S. H., Yang J. H., Choy J. H., Heterostructured nanohybrid of zinc oxide-montmorillonite clay. J. Phys. Chem. B. 2006; 110: 1599–1604. DOI: 10.1021/jp0543633

[11] Fatimah I., Wang, S., Wulandari D., ZnO/montmorillonite for photocatalytic and photochemical degradation of methylene blue. Appl. Clay Sci. 2011; 53: 553–560. DOI: 10.1016/j.clay.2011.05.001

[12] Meshram S., Limaye R., Ghodke S., Nigam S., Sonawane S., Chikate R., Continuous flow photocatalytic reactor using ZnO-bentonite nanocomposite for degradation of phenol. Chem. Eng. J. 2011; 172: 1008–1015. DOI: 10.1016/j.cej.2011.07.015

[13] Xu W. G., Liu S. F., Lu S. X., Kang S. Y., Zhou Y., Zhang H. F., Photocatalytic degradation in aqueous solution using quantum-sized ZnO particles supported on sepiolite. J. Colloid Interf. Sci. 2010; 351: 210–216. DOI: 10.1016/j.jcis.2010.07.052

[14] Bautista F. M., Campelo J. M., Luna D., Luque J., Marinas J. M., Vanadium oxides supported on TiO_2-sepiolite and sepiolite: Preparation, structural and acid characteri-

zation and catalytic behavior in selective oxidation of toluene. Appl. Catal. A: Gen. 2007; 325: 336–344. DOI: 10.1016/j.apcata.2007.02.033

[15] Arques A., Amat A. M., Santos-Juanes L., Vercher R. F., Marín M. L., Miranda M. A., Sepiolites as supporting material for organic sensitisers employed in heterogeneous solar photocatalysis. J. Mol. Catal. A: Chem. 2007; 27: 221–226. DOI: 10.1016/j.molcata.2007.02.038

[16] Suárez S., Yatez M., Petre A. L., Martin J. A., Avila P., Blanco J., Development of a new Rh/TiO_2-sepilote monolithic catalyst for N_2O decomposition. Appl. Catal. B: Environ. 2006; 64: 302–311. DOI: 10.1016/j.apcatb.2005.12.006

[17] Ökte A. N., Sayinsöz E., Characterization and photocatalytic activity of TiO_2 supported sepiolite catalysts. Separ. Purif. Technol. 2008; 62: 535–543. DOI: 10.1016/j.seppur.2008.03.011

[18] Portela R., Rubio-Marcos F., Leret P., Fernandez J. F., Banares M. A., Avilla P., Nanostructured ZnO/sepiolite monolithic sorbents for H_2S removal. J. Mater. Chem. A. 2015; 3: 1306–1316. DOI: 10.1039/C4TA04440A

[19] Anandan S., Vinu A., Sheeja Lovely K. L. P., Gokulakrishnan N., Srinivasu P., Mori T., Murugesan V., Sivamurugan V., Ariga K., Photocatalytic activity of La-doped ZnO for the degradation of monocrotophos in aqueous suspension. J. Mol. Cat. A. Chem. 2007; 266: 149–157. DOI: 10.1016/j.molcata.2006.11.008

[20] Lupan O., Chow L., Chai G., Roldan Cuenya B., Naitabdi A., Schulte A. A., Heinrich H., Nanofabrication and characterization of ZnO nanorod arrays and branched microrods by aqueous solution route and rapid thermal processing. Mater. Sci. Eng. B. 2007; 145: 57–66. DOI: 10.1016/j.mseb.2007.10.004

[21] Lupan O., Emelchenko G. A., Ursaki V. V., Chai G., Redkin A. N., Gruzintsev A. N., Tiginyanu I. M., Chow L., Ono L. K., Roldan Cuenya B., Heinrich H., Yakimov E. E., Synthesis and characterization of ZnO nanowires for nanosensor applications. Mater. Res. Bull. 2010; 45: 1026–1032. DOI: 10.1016/j.materresbull.2010.03.027

[22] Ökte A. N., Karamanis D., A novel photoresponsive ZnO-flyash nanocomposite for environmental and energy applications. Appl. Catal. B: Environ. 2013; 142–143: 538–552. DOI: 10.1016/j.apcatb.2003.12.008

[23] Ökte A. N., Karamanis D., Tuncel D., Dual functionality of TiO_2-flyash nanocomposites: Water vapor adsorption and photocatalysis. Catal. Today. 2014; 230: 205–213. DOI: 10.1016/j.cattod.2014.01.031

[24] Brunauer S., Deming L. S., Deming W. E, Teller E., On a theory of the van der Waals adsorption of gases. J. Am. Chem. Soc. 1940; 62: 1723–1732. DOI: 10.1021/ja01864a025

[25] Jing L., Xu Z., Sun X., Shang J., Cai W., The surface properties and photocatalytic activities of ZnO ultrafine particles. Appl. Surf. Sci. 2001; 180: 308–314. DOI: 10.1016/S0169-4332(01)00365-8

[26] Liqiang J., Dejun W., Baiqi W., Shudan L., Baifu X., Honggang F., Jiazhong S., Effects of noble metal modification on surface oxygen composition, charge separation and photocatalytic activity of ZnO nanoparticles. J. Mol. Catal. A. 2006; 244: 193–200. DOI: 10.1016/j.molcata.2005.09.020

[27] Sun H. Q., Feng X. H., Wang S. B., Ang H. M., Tadé M. O., Combination of adsorption, photochemical and photocatalytic degradation of phenol solution over supported zinc oxide: Effects of support and sulphate oxidant. Chem. Eng. J. 2011; 170: 270–277. DOI: 10.1016/j.cej.2011.03.059

[28] Lam S. M., Sin J. C., Abdullah A. Z., Mohamed A. R., Degradationof wastewaters containing organic dyes photocatalysedby zinc oxide: A review. Desalin. Water Treat. 2012; 41: 131–169. DOI: 10.1080/19443994.2012.664698

[29] Joseph J. M., Destaillats H., Hung H., Hoffmann M. R., The sonochemical degradation of azobenzene and related azo dyes:rate enhancements via Fenton's reactions. J. Phys. Chem. A. 2000; 104: 301–307. DOI: 10.1021/jp992354m

[30] Spadaro J. T., Isabelle L., Renganathan V., Hydroxyl radical mediated degradation of azo dyes: evidence for benzene generation. Environ. Sci. Technol. 1994; 28: 1389–1393. DOI: 10.1021/es00056a031

[31] Konstantinou K. I., Albanis T. A., TiO_2-assisted photocatalytic degradation of azo dyes in aqueous solution: kinetic and mechanistic investigations: A review. Appl. Catal. B: Environ. 2004; 49: 1–14. DOI: 10.1016/j.apcatb.2003.12.008